Journal of
Materials Chemistry C

Schottky Photodiodes Based on Mid-Wavelength Infrared Intraband Colloidal Quantum Dots – Surface Ligand and Metal Contact Studies

Journal:	*Journal of Materials Chemistry C*
Manuscript ID	TC-ART-02-2023-000648.R2
Article Type:	Paper
Date Submitted by the Author:	10-May-2023

Complete List of Authors:	Al Mahfuz, Mohammad Mostafa; New Jersey Institute of Technology, Department of Electrical and Computer Engineering Park, Junsung; New Jersey Institute of Technology, Department of Electrical and Computer Engineering Huebner, Rock; New Jersey Institute of Technology, Department of Mechanical and Industrial Engineering Lee, Sunghwan; Purdue University, School of Engineering Technology Ko, Dong-Kyun; New Jersey Institute of Technology, Department of Electrical and Computer Engineering

SCHOLARONE™
Manuscripts

Schottky Photodiodes Based on Mid-Wavelength Infrared Intraband Colloidal Quantum Dots – Surface Ligand and Metal Contact Studies

Mohammad M. Al Mahfuz[a], *Junsung Park*[a], *Rock Huebner*[b], *Sunghwan Lee*[c], *Dong-Kyun Ko*[a,*]

[a] Department of Electrical and Computer Engineering, New Jersey Institute of Technology, Newark, NJ 07102, United States

[b] Department of Mechanical and Industrial Engineering, New Jersey Institute of Technology, Newark, NJ 07102, United States

[c] School of Engineering Technology, Purdue University, West Lafayette, IN 47907, United States

* Corresponding author. E-mail address: dkko@njit.edu

†Electronic supplementary information (ESI) available.

Abstract: There is an emergent need for low-cost, uncooled detectors operating in the mid-wavelength infrared. Here, we report the first Schottky junction diode that utilizes intraband Ag_2Se

colloidal quantum dots as mid-wavelength infrared absorbers. These inexpensive, solution-processed Schottky devices exhibit orders-of-magnitude suppression of dark current compared to the photoconductors, while providing a greater fabrication simplicity compared to the barrier or p-n heterojunction devices. We highlight our findings on the role of the capping ligand in the detector performance parameters and discuss our metal contact studies to form rectifying junctions to the colloidal quantum dot films. The optimized Schottky devices show a favorable infrared responsivity of 0.1 A/W and an uncooled specific detectivity of 10^7 Jones. We also identify the present limitation of the device (1/f noise) and discuss potential paths toward future improvements.

Introduction

Materials absorb and emit thermal energies at different rates hence a region of interest whose temperature appears to be uniform is, in fact, made up of a mosaic of different temperatures. Thermal infrared sensors play an important role in offering this "heat signature" of natural, man-made, and biological objects with applications ranging from military surveillance, astronomy, environmental monitoring, and industrial processing control to medical diagnostics. The current market for high performance sensors is dominated by III-V superlattice, InSb, and HgCdTe devices in the mid-wavelength infrared (MWIR = 3 – 5 μm) and long-wavelength infrared (LWIR = 9 – 12 μm) spectral regions, despite their high cost and requirement for cryogenic cooling.[1,2] On the other hand, the demands for low-cost and uncooled options are entirely met by microbolometers, which perform well in the LWIR but poorly in the MWIR due to low responsivity and slow speed.[3] A significant effort is on the way to fill in this MWIR technology gap. While high operating temperature (HOT) infrared detectors based on epitaxial materials can significantly lower the cost by removing the need for cryogenic coolers, the overall price is still plagued by the high cost of

equipment – especially molecular beam epitaxy (MBE), expensive substrates, and slow film growth.[4] Recently, emerging devices based on nanomaterials including 2D materials such as graphene[5-8] as well as colloidal quantum dots (CQDs),[9-13] have provided a potential path toward low-cost, uncooled MWIR sensing. In particular, CQDs – which is the only available solution-processed materials option in the MWIR – are synthesized using facile benchtop chemistry and the photoresponsive film can be deposited directly on top of silicon read-out integrated circuits (ROICs) at the wafer scale. This enables the monolithic fabrication of focal plane arrays (FPAs) without the complexity of hybridization (indium bump bonding) required in traditional epitaxial technologies, thereby further reducing the manufacturing cost.[14]

Intraband CQDs are an emerging member of the semiconductor CQD materials family which are doped up to the first quantum confined energy levels ($1S_e$) and utilize the optical transitions between $1S_e$ and the second ($1P_e$) quantum confined energy levels. It has been studied that the Auger recombination process, which is a major obstacle that prevents narrow bandgap semiconductor detectors from reaching high sensitivity without cooling, is dramatically suppressed due to the sparse distribution of density of states.[15] This can allow high sensitivity MWIR photodetection at elevated temperatures, an exemplary example being lead salt (PbSe) detectors.[16] Ag_2Se intraband CQDs are a non-toxic alternative to HgSe CQDs[17,18], which have been demonstrated as photoconductive, barrier, and p-n heterojunction diode devices operating at room temperature,[19-21] while Schottky diodes have not been reported to date. In this work, we demonstrate MWIR Schottky photodiodes based on Ag_2Se CQDs which show reduced dark current, and noise compared to those of the photoconductors and allows simpler device fabrication compared to the barrier devices or p-n heterojunction diodes. We also report our findings on the

device performance as a function of varying CQD surface ligands and the contact metallization studies.

Experimental

Chemicals

Selenium (Se; Sigma-Aldrich, 99.999%), silver chloride (AgCl; Sigma-Aldrich, 99%), oleylamine (OLA; Sigma-Aldrich, 70%), trioctylphospine (TOP; Sigma-Aldrich, 90%), diphenylphosphine(DPP; Sigma-Aldrich, 98%), lead oxide (PbO; Sigma-Aldrich, 99.999%), hexamethyldisilathiane (TMS2S; Sigma-Aldrich, synthesis grade), oleic acid (OA; Sigma-Aldrich, 90%), 1-octadecene (ODE; Sigma-Aldrich, 90%), 1-butanol (Sigma-Aldrich 99.8%), hexane (Sigma-Aldrich, 98.5%), methanol (99.8%), octane (Sigma-Aldrich, 99%), ethyl alcohol (Sigma-Aldrich 99.5%), Acetonitrile (Thermo Scientific 99.5%), 1,2-ethanedithiol (EDT; Fluka, 98.0%), ammonium thiocyanate(NH4SCN; Sigma-Aldrich, 97.5%), 3-mercaptopropionic acid (MPA; Sigma-Aldrich, 99%), tetrabutylammonium iodide (TBAI; Sigma-Aldrich, 99%) and 1,3 -benzenedithiol (BDT; Sigma-Aldrich, 99%) were used as received.

Ag_2Se CQD Synthesis

Ag_2Se CQDs having an absorption peak around 4.5 μm were synthesized by following the previously reported standard hot-injection technique.[20,22] Briefly, in a glovebox filled with nitrogen, 1 M TOP-Se and 0.5M TOP-Ag precursor solutions were prepared separately by dissolving Se and AgCl respectively in trioctylphosphine (purity 90%). Under vacuum, 30 mL of oleylamine was heated to 90 °C in a three-neck flask for 1h. Next, switching the atmosphere to nitrogen, 8 mL of 1 M TOP−Se was added to oleylamine, and the temperature was raised to 135 °C. When the temperature reached 135 °C, 16 mL of 0.5 M TOP−Ag mixed with 800 μL DPP was

injected to initiate a reaction. To terminate the reaction after 20s, 20ml of butanol was injected to the mixture and it is subsequently cooled in a water bath to room temperature. The CQDs were precipitated by centrifugation with a mixture of methanol and ethanol. Then after three methanol washes, CQDs were dispersed in hexane/octane. The solution was then stored in a vial with a concentration of 40 mg/mL for further use.

PbS CQD Synthesis

The synthesis of PbS CQD with an absorption peak around 1000nm was performed based on the previously developed protocol.[23,24] First, in a three-neck flask a mixture of 0.45 g of lead oxide, 10 mL of 1-octadecene, and 2 mL of oleic acid was mixed and heated under vacuum to 110 °C for 2 h. In a separate vial, the sulfur precursor solution was prepared by mixing 0.2 mL of hexamethyldisilathiane and 5 mL of anhydrous 1-octadecene. This precursor solution was then quickly injected into the reaction flask under nitrogen environment at 110 °C. As a result, the mixture instantly turned from clear to dark, indicating a rapid nucleation. The reaction mixture was then cooled down naturally. Finally, the CQDs were precipitated using acetone by centrifugation inside nitrogen filled a glovebox and the final CQDs were dispersed in hexane/octane (40 mg/mL).

Device Fabrication

Devices were fabricated on glass substrates (10 × 10 mm) after cleaning them by sonication with isopropyl alcohol, acetone, and hexane. After drying the substrates with N_2 flow, 40nm bottom contacts (Cr/Au or Cr/Al) were deposited using thermal evaporation using a shadow mask with a deposition rate around 1 Å/s under a vacuum of 2×10^{-6} mbar. By mixing the desired amount of Ag_2Se and PbS CQD solutions (optimized mixture ratio: 50 µL of Ag_2Se CQD and 750 µL PbS CQD solution) and stirring with a vortex machine for 60 s, the binary CQDs solution was prepared.

The solution was then deposited on the substrates via spin coating at 2000 rpm for 30s layer by layer (up to 8 layers). After each layer the substrate was dipped into the desired ligand exchange solution for 20s and rinsed with acetonitrile for 20s. Acetonitrile was used as the solvent for preparing the ligands exchange solutions, the concentrations were as follows, 1,2-ethanedithiol (EDT) 10mM, ammonium thiocyanate (for SCN) 100mM, 3-mercaptopropionic acid 50mM, tetrabutylammonium iodide (TBAI) 10mg/ml, and 1,3 -benzenedithiol (BDT) 1.7mM. After the film deposition, a top contact (Au-70nm) was deposited using a shadow mask through thermal evaporation defining a 200 μm × 200 μm device area. The fabrication was completed by cleaning the CQDs near the bottom contact to expose the contact pad using a wooden tip.

Device Characterization

Device characterizations were carried out using a calibrated blackbody (900 °C, Newport 67030) as an illumination source. The light was modulated using an optical chopper at 15 Hz and filtered through 4.5 μm band pass filter. The photocurrent was measured using a lock-in technique with SR570 preamplifier and SR 830 lock-in amplifier. The preamplifier also provided the bias to the device. The responsivity (mA/W) was calculated by dividing measured photocurrent (mA) with the optical power calculated for 4.5 μm filter (0.65 μW, after correcting for source aperture, optical pass, optics, and detector area). For the spectral responsivity measurements, 4.5 μm filter was replaced with a set of band-pass filters with center wavelengths varying from 2.5–6 μm. All measurements were done at room temperature without cooling. The device dark resistance was calculated from the current-voltage (I-V) characteristics that were measured using Agilent 4155A semiconductor parameter analyzer.

Dark current noise was measured at 300K using a SR570 preamplifier to amplify the noise spectrum and was recorded using a SR760 Fast Fourier Transform spectrum analyzer. Bias

voltages were applied to the devices using the preamplifier's internal battery and Faraday shielded boxes were used to isolate the external noise sources in the lab environment.

Results And Discussion

Binary CQD Study

The heavily-doped nature of Ag_2Se intraband CQDs presents difficulties in realizing a Schottky barrier with metals because it will electrically form a tunneling contact (Ohmic). In our previous study,[19] we have proposed a binary CQD approach to overcome this issue and a similar approach is utilized here. Specifically, we form a binary mixture of intraband Ag_2Se CQDs and intrinsic PbS CQDs to reduce the overall mobile carrier concentration in the film where the transport of ground state electrons and holes are blocked due to the energetic position of the Ag_2Se CQDs with respect to PbS CQDs, as depicted in Fig. 1(a,b). The transport of photoexcited electrons in the Ag_2Se CQDs, on the other hand, remains unimpeded, thereby allowing the generation of photocurrents (Fig. 1(c)).

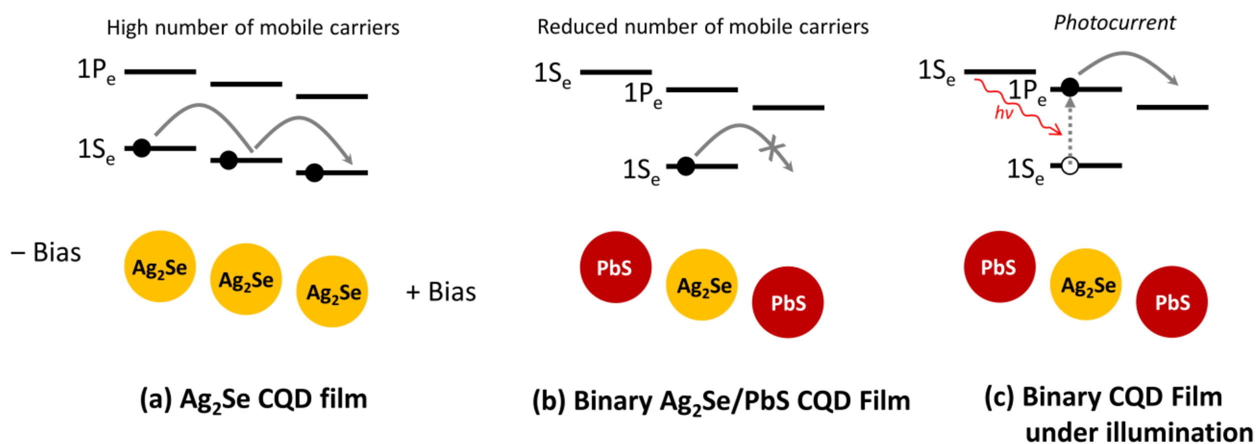

Fig. 1 Schematic depiction of (a) Ag_2Se CQD film, (b) binary Ag_2Se/PbS mixture film, and (c) binary Ag_2Se/PbS mixture film under infrared illumination.

First, the CQD samples, average size of 3 nm PbS and 5.5 nm Ag_2Se CQDs were synthesized (see Fig. 2(a) and 2(b)). The optical absorption of CQDs were obtained using Fourier transform infrared (FTIR), as shown in Fig. 2(c) and 2(d). A broad absorption peak around 3 – 6 μm shown in Fig. 2(c)[25]arises from the intraband absorption Ag_2Se CQDs. Fig. 2(d) shows the FTIR spectrum of PbS CQDs, which shows an absence of optical absorption in the MWIR. Sharp peaks around 3.4 μm arise from the vibrational signatures of C-H. Using these two types of CQDs, we have prepared the optimized CQD mixture solution sample corresponding to 50/750 Ag_2Se/PbS volume ratio (see Supplementary Information S1).[26]

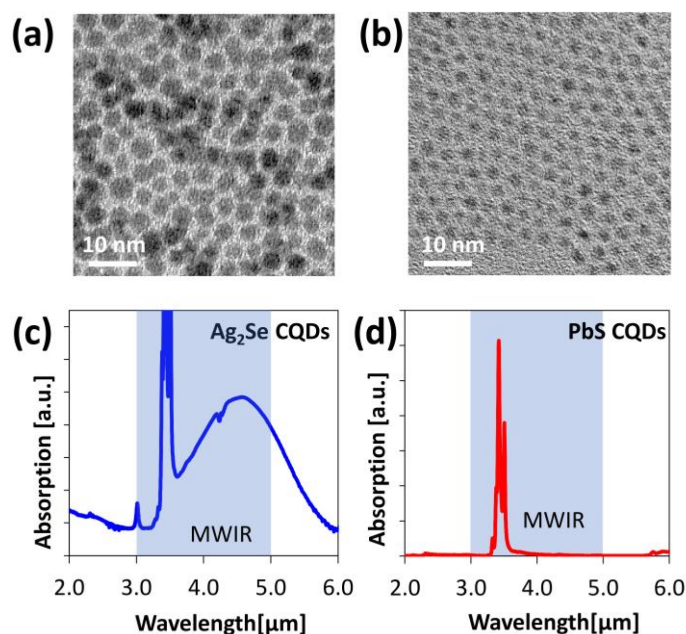

Fig. 2 Optical absorption of (a) Ag_2Se CQD and (b) PbS CQD obtained using FTIR measurement. Sharp peaks around 3.4 μm arise from the vibrational signatures of C-H.

Effect of Ligands on Binary CQD Device Performance

The performance of any CQD-based devices is known to be highly sensitive to the surface capping ligands. Hence CQD ligand studies were conducted prior to Schottky device studies. The type of

ligands investigated are 1,2-ethandithiol (EDT),[27,28] 1,3-benzenedithiol (BDT),[29,30] 3-mercaptopropionic acid (MPA),[31,32] ammonium thiocyanate (SCN),[33] and tetrabutylammonium iodide (TBAI).[34] EDT and BDT serve as a standard, compact organic ligands and MPA, SCN, and TBAI were selected due to their reports of high photodetector, solar cell, and transistor performances.

To identify the best performing CQD ligands, we have fabricated vertically-stacked devices to measure two key detector performance parameters: MWIR responsivity and dark resistivity. First, to fabricate the device, a Cr/Au bottom contact is formed on a glass substrate using a shadow mask and thermal evaporation. Then, a total of 8 layers of binary CQD film (~ 120 nm) is deposited using a layer-by-layer spin-coating and ligand-exchange method. The device is completed with a 70 nm top contact Au layer deposited using a shadow mask and thermal evaporation. This top contact forms a 'via opening' that allows infrared radiation to illuminate the binary CQD film – a common design found in many up-ward looking MWIR devices[35] and standard silicon solar cells (top finger electrodes). A device schematic is shown in Fig. 3(a). The infrared responsivity of the device was characterized using a lock-in technique with a calibrated blackbody illuminated through a 4.5 μm bandpass filter serving as radiation source. A series of identical devices were fabricated, except the CQD films were ligand-exchanged with various ligands (see Supplementary Information S2). During the course of measurements, it was noted that the devices made from different ligands have different maximum biases that can be applied, exceeding the maximum bias leads to irreversible degradation of the device. Hence, a low bias of 0.9 V was used for all devices for responsivity comparison. Fig. 3(b) and 3(c) shows the device responsivity and dark resistivity, respectively.

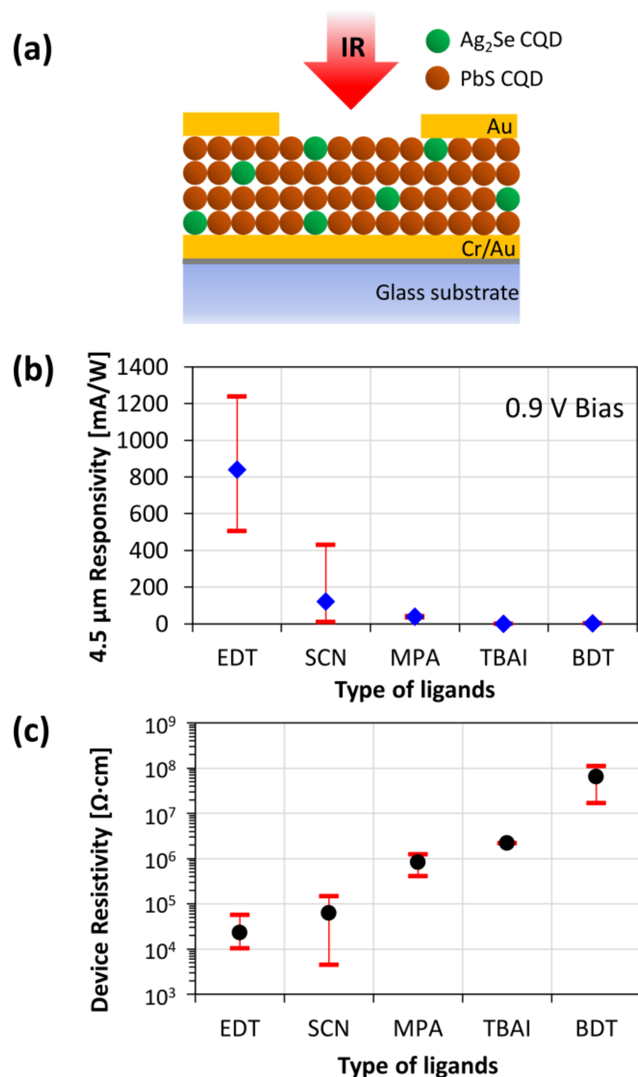

Fig. 3 (a) Device schematic of upward-looking, vertically-stacked binary CQD device, (b) plot of 4.5 µm peak responsivity with varying ligands used for CQD film ligand-exchange, and (c) plot of device dark resistivity with varying ligands.

The analysis of the Fig. 3 data reveals a trend: for the devices with higher electrical conductivities (lower resistivity), higher responsivities are observed, except for the TBAI devices which showed zero photoresponse at 0.9 V. This can be understood based on the relationship that both the magnitude of dark current and the photocurrent is proportional to the carrier mobility. The trend observed here points to the fact that the predominant effect of the ligand-exchange is the

change in the carrier mobility of the CQD film. While ligand-exchange can induce changes in the carrier lifetime due to improved/degraded surface defect passivation, the changes are typically small (less than 3-times),[32,36,37] compared to the orders of magnitude difference observed in Fig. 3(b) and 3(c). The size of the ligand determines the interparticle distance and the carrier mobility (μ) of the CQD film has an exponential dependence on the inverse of interparticle distance, given by

$$\mu = \mu_0 \exp(-\beta d) \exp\left(-\frac{\Delta E}{kT}\right)$$

where, μ_0 is the mobility prefactor, β is the tunneling decay constant, d is the interparticle distance, ΔE is the transport energy level variation, k is the Boltzmann constant, and T is the temperature. The order of ligand size studied here is: TBAI (I^- atomic ligand) < SCN (inorganic SCN^- ligand) < EDT (C2-SH) ≤ MPA (C2-COOH) < BDT (most bulky in size). While EDT and MPA have the same C2 chain (two carbon backbones), MPA has carboxylic acid on the other end giving rise to a different surface binding configuration and this might be the reason for the larger interparticle distance observed in this binary CQD study. With the exception of TBAI and SCN, the device resistivity follows the ligand size trend (EDT < MPA < BDT), as shown in Fig. 4(a). The exception of TBAI and SCN occurs due to Schottky contact formation (see Fig. 4(b) and Supplementary Information S4). EDT, MPA, and BDT form Ohmic or quasi-Ohmic contacts while TBAI and SCN form Schottky contacts to the Au metal electrodes, therefore showing higher-than-anticipated device resistivity. The energetic position of the conduction and valence level of CQDs has been reported previously to vary with the type of surface ligands.[38] The report is consistent with the results obtained here that TBAI and SCN have deeper lying energy levels compared to EDT and MPA (as much as 0.5 eV), thereby forming a Schottky barrier for holes in contact with

Au. If the Schottky contacts are formed both at the top and bottom of the CQD film, this would create a back-to-back diode (one diode in opposite polarity to the other). However, Fig. 4(b) shows the typical characteristics of a single rectifying diode, indicating that the metal-CQD contact formed at the bottom and the CQD-metal contact formed at the top are different, despite using identical metal material. This arises from the fact that, for the bottom contact, CQDs are mildly solution-deposited on top of metal electrode whereas, for the top contacts, metals are thermally deposited on CQD film; during metal evaporation, the underlying CQD film may be damaged creating defects. This would lead to Fermi level pinning, thereby creating an Ohmic contact irrespective of the type of metal deposited. Device resistivity data shown in Fig. 3(c) was extracted from the reverse (negative) bias region, as this region typically used for the operation photodetector, due to the low dark current.

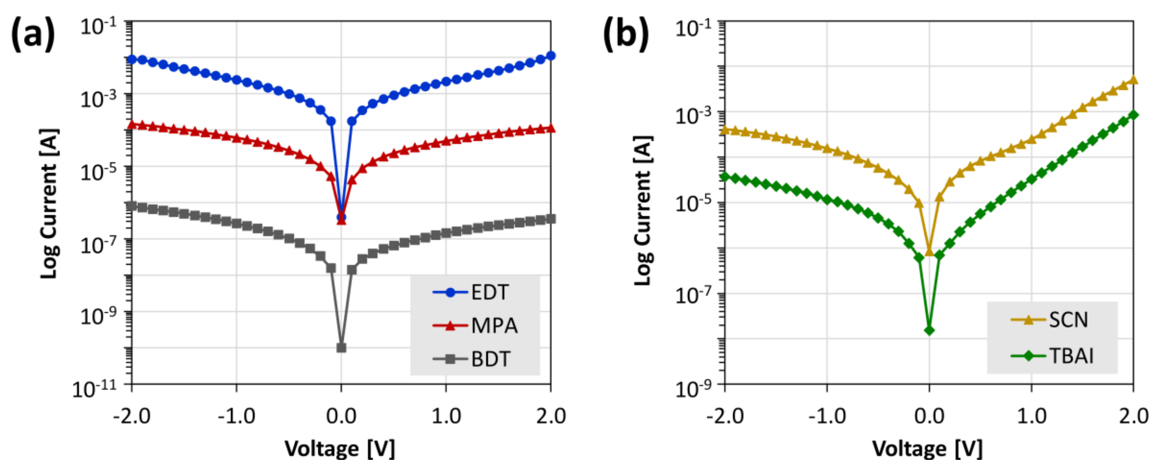

Fig. 4 Current-voltage (I-V) characteristics of (a) various organic and (b) inorganic ligands investigated in this study plotted in logarithmic current scale.

Schottky Diodes

In this study in terms of determining the optimum ligand, EDT was identified to show the highest infrared responsivity. However, it was noted the EDT devices suffer from high dark current. The

dark current typically determines the magnitude of current noise and it is a major limiting factor for achieving high specific detectivity. As discussed previously, the fact that dark resistivity and responsivity are interrelated through carrier mobility makes it challenging to maximize the detector sensitivity by modifying the material properties (binary mixture ratios and ligands) alone. Thus, to further improve the detector performance, modification of the device structure is sought. Specifically, since the primary source of dark current in a photoconductive device is the majority carrier drift current, the formation of a Schottky contact barrier will block the flow of majority carriers, thereby significantly reducing the dark current. To fabricate this Schottky diode device, every processing parameter was kept identical except that the Au bottom contact (work function = 5.2 eV) was replaced with low work function Al (work function = 4.1 eV). Based on the lesson learned from the previous ligand optimization study, a Schottky contact was formed at the bottom electrode instead of the top which may create Fermi pinning. Fig. 5(a,b) shows current-voltage (I-V) characteristics comparison of a photoconductor (Au-EDT CQD-Au device) and a Schottky diode (Al-EDT CQD-Au device). A strong rectifying characteristic with an on/off ratio of 2.1×10^{2} (± 2V) was observed due to the Al-binary CQD Schottky barrier formation. Compared to the photoconductor, the Schottky diode exhibit a three orders of magnitude reduction in the dark current (under reverse bias) while the magnitude of the 4.5 um peak responsivity (Fig. 5(c)) was only reduced by approximately 6-times. This results in about two orders of magnitude increase in the sensitivity ratio (SR), defined as SR = I_{photo}/I_{dark}, from 2.4×10^{-4} (Photoconductor) to 3.6×10^{-2} (Schottky). This EDT ligand-based Schottky diode also outperforms the SCN and TBAI Schottky diodes unintentionally fabricated previously in Fig. 4(b) ($SR_{SCN} = 1.4 \times 10^{-4}$, $SR_{TBAI} \approx 0$). The spectral response plot shown in Fig. 5(c) also shows close resemblance to the optical absorption spectrum obtained from Ag_2Se CQDs, indicating that the device photoresponse arise from

photocarriers generated from Ag_2Se CQDs and not from a bolometric effect (which exhibits flat spectral response[39]).

The reduction in dark current observed in the Schottky diode should translate to a reduction in the current noise. Fig. 5(d) shows the current noise spectral density comparison of the photoconductor and the Schottky diode. At 15 Hz, our responsivity measurement frequency, the Schottky diode exhibited 1.34×10^{-10} $A \cdot Hz^{-1/2}$ of current noise compared to 8.47×10^{-9} $A \cdot Hz^{-1/2}$ of a photoconductor, which is about a 60-fold reduction. A close examination of the current noise spectra as a function of frequency shows that it follows an inverse power law with an exponent of 0.73, indicating that 1/f is the dominant source of noise. In Fig. 5(d), calculated shot noise obtained using the equation $i_n^{shot} = \sqrt{2qI_{dark}}$, where q is the fundamental charge and I_{dark} is the device dark current, and calculated Johnson noise using equation $i_n^{Johnson} = \sqrt{4kT/R}$, where k is the Boltzmann constant, T is the temperature, and R is the device DC resistance, are also overlaid. While in single crystalline devices, other noise mechanisms, such as shot noise or Johnson noise, are often the dominant noise mechanisms, in CQD devices, 1/f noise shows a dominant contribution over wide range of frequencies[40] and is consistent with this data (1/f knee exceeding 10 KHz). This 1/f noise has been studied to originate from the granular nature of the material and is independent of the chemical composition of the CQD material; metal, semiconductor, wide-bandgap insulator CQDs all show the similar 1/f noise behavior.[41]

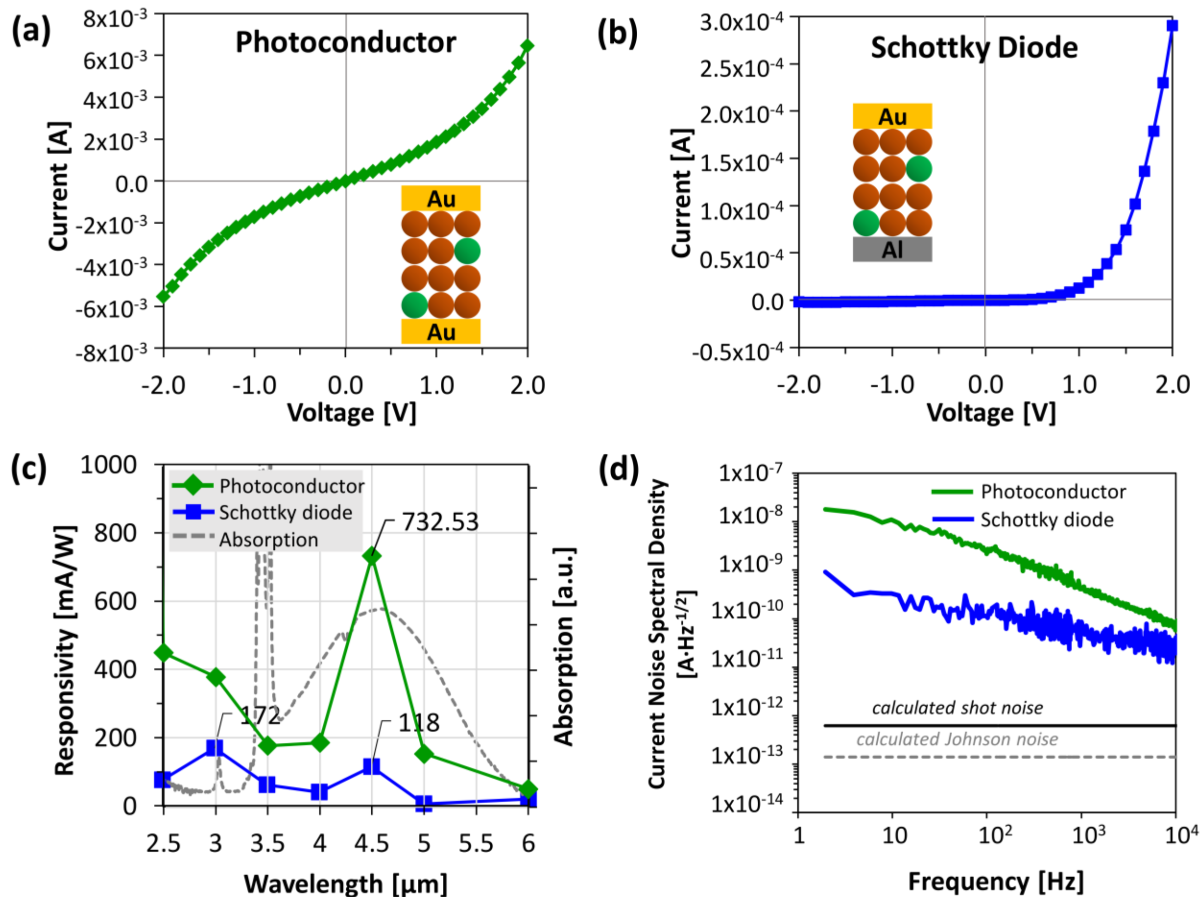

Fig. 5 Current-voltage plot of (a) Au-EDT CQD-Au photoconductor and (b) Al-EDT CQD-Au Schottky diode. (c) shows the spectral responsivity comparison. The optical absorption spectrum of Ag_2Se CQD is overlaid for reference. (d) shows the current noise spectral density as a function of frequency. Calculated shot noise (6.18×10^{-13} $A \cdot Hz^{-1/2}$) and Johnson noise current (1.40×10^{-13} $A \cdot Hz^{-1/2}$) are overlaid as a reference to the Schottky diode data.

Performance Comparison

The ultimate figure of merit of a photodetector is the specific detectivity (D^*). Based on the responsivity and current noise measured above, the room temperature D^* of our binary CQD Schottky diode is calculated to be 1.5×10^7 Jones ($cm \cdot Hz^{1/2}/W$) at its 4.5 μm peak(NEP = 1.3×10^{-9} $W/Hz^{-1/2}$). The comparison of detector performance parameters with other technologies

(commercial product and leading research) is summarized in Table 1. The current leading-research is based on HgTe CQD p-n junction devices,[42] where the peak responsivity is about 2–3 times lower but show 10^2-times better noise performance and the D^* is about one order of magnitude higher. Commercial epitaxial HgCdTe (Thorlab VL5T0)[43] is the most mature technology and currently outperforms all CQD technologies, but it suffers from expensive material growth and high cost of focal plane array fabrication. It is also worth noting that the epitaxial HgCdTe and HgTe CQD devices were optically enhanced while our Schottky diode devices have no optical enhancement implemented. Overall, the binary CQD Schottky diode devices studied in this work show approximately 10^7 Jones of detectivity at room temperature. While the infrared responsivity compares favorably with other technologies, its main limitation is the high current noise arising from 1/f source.

Table 1. Comparison of room temperature device performance parameters of binary CQD Schottky diode (this work) with commercial and leading research photovoltaic technologies. PV stands for photovoltaic.

Detector Material	Device Type	Temp.	Peak λ	Peak R	Current Noise	Detectivity at peak	Note
HgTe CQD[42]	PV (p-n junction)	300 K	3.8 μm	0.05 A/W	3.5×10^{-12} $A \cdot Hz^{-1/2}$ * (Device area 2×10^{-4} cm^2)	2.0×10^8 Jones	Optical spacer enhancement
Epitaxial HgCdTe[43]	PV (Thorlab VL5T0)	300 K	5 μm	> 1 A/W	6.6×10^{-12} $A \cdot Hz^{-1/2}$ * (Device area 1×10^{-2} cm^2)	1.5×10^{10} Jones	Optically immersed lens (hyper-hemi spherical GaAs)
Binary CQD (this work)	PV (Schottky diode)	300 K	3 μm, 4.5 μm	0.17 A/W, 0.11 A/W	1.34×10^{-10} $A \cdot Hz^{-1/2}$ (Device area 4×10^{-4} cm^2)	2.5×10^7 Jones, 1.5×10^7 Jones	No optical enhancements

* The current noise values for epitaxial HgCdTe and HgTe CQD were estimated from the detectivity and responsivity values.

The low-temperature behavior of our devices has yet to be studied. In HgTe QD photovoltaic device research, cooling has been studied to improve both the responsivity and current noise. Specifically, cooling from 300 K to 100 K leads to an 8-times improvement in the responsivity (from 0.05 A/W to 0.42 A/W) and causes a two orders of magnitude reduction in the current noise (from 3.5×10^{-12} $A \cdot Hz^{-1/2}$ to 5.9×10^{-14} $A \cdot Hz^{-1/2}$), ultimately resulting in a 10^3-times increase in specific detectivity (from 2.0×10^8 Jones to 1.0×10^{11} Jones).[42] If our binary CQD Schottky device exhibit similar improvements, this will lead to > 10^{10} Jones at ≈ 100K. In fact, we anticipate higher performance gains through cooling, because the major constituent of our binary CQD is PbS CQDs and the energy gap of PbS CQD (1.12 eV) is much larger than HgTe CQD (0.25 eV).

Conclusion

In summary, we demonstrate MWIR Schottky photodiodes based on binary CQD film composed of intraband Ag_2Se CQDs and PbS CQDs. Among the various capping ligands studied, EDT shows the high infrared responsivity and the introduction of a Schottky barrier using Al contact suppresses the current noise down by an order of magnitude, leading to a detectivity D^* of 10^7 Jones at room temperature.

Along with the cooling discussed previously, further materials and device research can be conducted to improve the performance. In CQD solar cell research, it has been demonstrated that the use of hybrid ligands[44-46] improves both the CQD film mobility and surface passivation. It is anticipated that similar strategy can be implemented to MWIR CQD detectors. In a device perspective, the current Schottky diode can be further improved by inserting a thin passivation

layer between the metal and CQD layer (known as metal-insulator-semiconductor or MIS device).[46] Suppression of dark current and current noise is anticipated that may lead to higher detectivity.

AUTHOR INFORMATION

Corresponding Author

Dong-Kyun Ko − Department of Electrical and Computer Engineering, New Jersey Institute of Technology, Newark, New Jersey 07102, United States; orcid.org/0000-0003- 1834-0241; Email: dkko@njit.edu

Authors

Mohammad M. Al Mahfuz − Department of Electrical and Computer Engineering, New Jersey Institute of Technology, Newark, New Jersey 07102, United States

Junsung Park − Department of Electrical and Computer Engineering, New Jersey Institute of Technology, Newark, New Jersey 07102, United States

Rock Huebner − Department of Mechanical and Industrial Engineering, New Jersey Institute of Technology, Newark, NJ 07102, United States

Sunghwan Lee − School of Engineering Technology, Purdue University, West Lafayette, Indiana 47907, United States; orcid.org/0000-0001-6688-8995

ACKNOWLEDGEMENT

Research Sponsored by SBIR Funding Office of Naval Research Contract No. N68335-22-C-0079. The approved Document Control Number (DCN #): 43-10152-22.

References

1 M. Henini and M. Razeghi, *Handbook of Infrared Detection Technologies*, Elsevier Sciences Inc, New York, 2002.

2 A. Rogalski, *Infrared Phys. Technol.*, 2011, 54, 136−154.

3 M. E. Cryer and J. E. Halpert, *ACS Photonics,* 2018, 5, 8, 3009–3015

4 J. Qiu, Y. Liu, Z. Cai, Q. Phan, Z. Shi, Mater. Adv., 2022, 3, 1079–1086

5 A. Rogalski, *Adv. Opt. Photonics,* 2019, 2, 314–379

6 M. S. Shawkat, S. B. Hafiz, M. M. Islam, S. A. Mofid, M. M. Al Mahfuz, A. Biswas, H.-S. Chung, E. Okogbue, T.-J. Ko, D. Chanda, T. Roy, D.-K. Ko and Y. Jung, *ACS Appl. Mater. Interfaces,* 2021, 13, 15542–15550.

7 W. Yan, V. R. Shresha, Q. Jeangros, N. S. Azar, S. Balendhran, C. Ballif, K. Crozier and J. Bullock, *ACS Nano,* 2020, 14, 13645–13651.

8 Y. Fang, Y. Ge, C. Wang and H. Zhang, *Laser & Photonics Rev.,* 2020, 14,1, 1900098.

9 A. Rogalski, P. Martyniuk, M. Kopytko and W. Hu, *Appl. Sci.,* 2021, 11, 501.

10 C. Melnychuk and P. Guyot-Sionnest, *J. Electron. Mater.,* 2022, 51, 1428–1435.

11 M. Chen, G. Shen and P. Guyot-Sionnest, *J. Phys. Chem. C*, 2020, 124, 29, 16216–16221.

12 T. H. Dang, C. Abadie, A. Khalili, C. Gréboval, H. Zhang, Y. Prado, X. Z. Xu, D. Gacemi, A. Descamps-Mandine, S. Ithurria, Y. Todorov, C. Sirtori, A. Vasanelli and E. Lhuillier, *Adv. Opt. Mater.,* 2022, 10, 9, 2200297.

13 A. Khalili, M. Weis, S. G. Mizrahi, A. Chu, T. H. Dang, C. Abadie, C. Gréboval, C. Dabard, Y. Prado, X. Z. Xu, E. Péronne, C. Livache, S. Ithurria, G. Patriarche, J. Ramade, G. Vincent, D. Boschetto and E. Lhuillier, *ACS Photonics,* 2022, 9, 985–993.

14 S. B. Hafiz, M. Scimeca, A. Sahu and D.-K. Ko, Nano Convergence, 2019, 6, 7.

15 C. Melnychuk and P. Guyot-Sionnest, *ACS Nano,* 2019, 13, 10512–10519.

16 J. Qiu, Y. Liu, Z. Cai, Q. Phan and Z. Shi, *Mater. Adv.,* 2022, 3, 1079–1086.

17 C. Livache, B. Martinez, N. Goubet, C. Gréboval, J. Qu, A. Chu, S. Royer, S. Ithurria, M. G. Silly, B. Dubertret and E. Lhuillier, *Nat. Commun.*, 2019, 10, 2125.

18 X. Tang, G. fu -Wu and K. W. C. Lai, J. Mater. Chem. C, 2017, 5, 362–369.

19 S. B. Hafiz, M. R. Scimeca, P. Zhao, I. J. Paredes, A. Sahu and D.-K. Ko, *ACS Appl. Nano Mater.,* 2019, 2, 1631–1636.

20 S. B. Hafiz, M. M. Al Mahfuz and D.-K. Ko, *ACS Appl. Mater. Interfaces,* 2021, 13, 937–943.

21 S. B. Hafiz, M. M. Al Mahfuz, S. Lee and D.-K. Ko, *ACS Appl. Mater. Interfaces,* 2021, 13, 49043–49049.

22 A. Sahu, A. Khare, D. D. Deng and D. J. Norris, *Chem. Comm.,* 2012, 48, 5458–5460.

23 J. Zhang, R. W. Crisp, J. Gao, D. M. Kroupa, M. C. Beard and J. M. Luther, *J. Phys. Chem. Lett.,* 2015, 6, 1830–1833.

24 M. A. Hines and G. d. Scholes, *Advanced Materials*, 2003, 15, 1844–1849.

25 M. Park, D. Choi, Y. Choi, H. Shin and K. S. Jeong, *ACS Photonics,* 2018, 5, 1907–1911.

26 M. Cargnello, A. C. Johnston-Peck, B. T. Diroll, E. Wong, B. Datta, D. Damodhar, V. V. T. Doan-Nguyen, A. A. Herzing, C. R. Kagan and C. B. Murray, *Nature,* 2015, 524, 450–453.

27 J. M. Luther, M. Law, Q. Song, C. L. Perkins, M. C. Beard and A. J. Nozik, *ACS Nano,* 2008, 2, 271–280.

28 Y. Liu, M. Gibbs, J. Puthussery, S. Gaik, R. Ihly, H. W. Hillhouse and M. Law, *Nano Lett.,* 2010, 10, 1960–1969.

29 G. I. Koleilat, L. Levina, H. Shukla, S. H. Myrskog, S. Hinds, A. G. Pattantyus-Abraham and E. H. Sargent, *ACS Nano,* 2008, 2, 833–840.

30 K. Szendrei, W. Gomulya, M. Yarema, W. Heiss and M. A. Loi, *Appl. Phys. Lett.,* 2010, 97, 203501.

31 A. Maulu, J. Navarro-Arenas, P. J. Rodríguez-Cantó, J. F. Sánchez-Royo, R. Abargues, I. Suárez and J. P. Martínez-Pastor, *Nanomaterials,* 2018, 8, 677.

32 K. S. Jeong, J. Tang, H. Liu, J. Kim, A. W. Schaefer, K. Kemp, L. Levina, X. Wang, S. Hoogland, R. Debnath, L. Brzozowski, E. H. Sargent and J. B. Asbury, *ACS Nano,* 2012, 6, 89–99.

33 J.-H. Choi, A. T. Fafarman, S. J. Oh, D.-K. Ko, D. K. Kim, B. T. Diroll, S. Muramoto, J. G. Gillen, C. B. Murray and C. R. Kagan, *Nano Lett.,* 2012, 12, 2631–2638.

34 J. Tang, K. W. Kemp, S. Hoogland, K. S. Jeong, H. Liu, L. Levina, M. Furukawa, X. Wang, R. Debnath, D. Cha, K. W. Chou, A. Fischer, A. Amassian, J. B. Asbury and E. H. Sargent, *Nat. Mater.,* 2011, 10, 765–771.

35 K.-A. Son, D. Wong, H. Sharifi, H. C. Seo, T. De Lyon, S. Terterian, J. S. Moon and T. Hussain, *IEEE Trans. on Nanotechnol.y,* 2015, 14, 10–14.

36 B. Martinez, C. Livache, N. Goubet, A. Jagtap, H. Cruguel, A. Ouerghi, E. Lacaze, M. G. Silly and E. Lhuillier, *J. Phys. Chem. C*, 2018, 122, 859–865.

37 G. H. Carey, L. Levina, R. Comin, O. Voznyy and E. H. Sargent, *Adv. Mater.,* 2015, 27, 3325–3330.

38 P. R. Brown, D. Kim, R. R. Lunt, N. Zhao, M. G. Bawendi, J. C. Grossman and V. Bulović, *ACS Nano*, 2014, 8, 5863–5872.

39 A. Rogalski, *Opto−Electro Rev.* 2012, 20, 279–308

40 A. De Iacovo, C. Venettacci, L. Colace, L. Scopa and S. Foglia, *Appl. Phys. Lett.,* 2017, 111, 211104.

41 H. Liu, E. Lhuillier and P. Guyot-Sionnest, *J. Appl. Phys.,* 2014, 115, 154309.

42 M. M. Ackerman, X. Tang and P. Guyot-Sionnest, *ACS Nano,* 2018, 12, 7264–7271.

43 Thorlabs - VL5T0 HgCdTe Single-Junction Photovoltaic Detector, 5.0 µm, 1 mm² Active Area, https://www.thorlabs.com, (accessed 9 February 2023).

44 A. H. Ip, S. M. Thon, S. Hoogland, O. Voznyy, D. Zhitomirsky, R. Debnath, L. Levina, L. R. Rollny, G. H. Carey, A. Fischer, K. W. Kemp, I. J. Kramer, Z. Ning, A. J. Labelle, K. W. Chou, A. Amassian and E. H. Sargent, *Nat. Nanotechnol.*, 2012, 7, 577–582.

45 J. Zhang, J. Gao, C. P. Church, E. M. Miller, J. M. Luther, V. I. Klimov and M. C. Beard, *Nano Lett.,* 2014, 14, 6010–6015.

46 Y. Yang, B. Zhao, Y. Gao, H. Liu, Y. Tian, D. Qin, H. Wu, W. Huang and L. Hou, *Nano-Micro Lett.,* 2015, 7, 325–331.

47 C.-H. Lin and C. W. Liu, *Sensors,* 2010, 10, 8797–8826.